Metallomics

PAPER

View Article Online
View Journal | View Issue

Cite this: *Metallomics*, 2017, 9, 1073

Mechanisms of iron and copper–frataxin interactions†

T. H. L. Han,[a] J. M. Camadro,[b] R. Santos,[‡b] E. Lesuisse,[b] J. M. El Hage Chahine[a] and N. T. Ha-Duong[*a]

Received 3rd February 2017,
Accepted 9th May 2017

DOI: 10.1039/c7mt00031f

rsc.li/metallomics

Frataxin is a mitochondrial protein whose deficiency is the cause of Friedreich's ataxia, a hereditary neurodegenerative disease. This protein plays a role in iron–sulfur cluster biosynthesis, protection against oxidative stress and iron metabolism. In an attempt to provide a better understanding of the role played by metals in its metabolic functions, the mechanisms of mitochondrial metal binding to frataxin *in vitro* have been investigated. A purified recombinant yeast frataxin homolog Yfh1 binds two Cu(II) ions with a $K_{d1}(Cu^{II})$ of 1.3×10^{-7} M and a $K_{d2}(Cu^{II})$ of 3.1×10^{-4} M and a single Cu(I) ion with a higher affinity than for Cu(II) ($K_d(Cu^{I}) = 3.2 \times 10^{-8}$ M). Mn(II) forms two complexes with Yfh1 ($K_{d1}(Mn^{II}) = 4.0 \times 10^{-8}$ M; $K_{d2}(Mn^{II}) = 4.0 \times 10^{-7}$ M). Cu and Mn bind Yfh1 with higher affinities than Fe(II). It is established for the first time that the mechanisms of the interaction of iron and copper with frataxin are comparable and involve three kinetic steps. The first step occurs in the 50–500 ms range and corresponds to a first metal uptake. This is followed by two other kinetic processes that are related to a second metal uptake and/or to a change in the conformation leading to thermodynamic equilibrium. Frataxin deficient *Δyfh1* yeast cells exhibited a marked growth defect in the presence of exogenous Cu or Mn. Mitochondria from *Δyfh1* strains also accumulated higher amounts of copper, suggesting a functional role of frataxin *in vivo* in copper homeostasis.

Introduction

Friedreich's ataxia (FA) is the most common autosomal recessive cerebrospinal ataxia in Caucasian populations. It is caused in the majority of patients by the expansion of a homozygous GAA triplet repeat in the first intron of the gene encoding frataxin. This mutation leads to an alteration of gene transcription, which results in a decrease in the expression of frataxin. The disease is characterized by a combination of neuropathy, cardiomyopathy, glucose metabolism disturbances and skeletal abnormalities.[1] These are thought to be the consequences of mitochondrial defects related to respiratory deficiency, oxidative stress condition, and possibly to an alteration of iron metabolism. Although the involvement of frataxin in FA is well documented, the specific function of the protein remains a matter of debate. It has been shown in human cells, *Saccharomyces cerevisiae* and other model organisms that frataxin can either serve as a chaperone protein that binds iron or play a role in regulating Fe–S cluster biosynthesis as part of a protein complex with the cysteine desulfurase Nfs1, the scaffold protein Isu1 and the accessory protein Isd11, or even facilitate heme biosynthesis.[2–5] It is interesting to note that one of the common features of the frataxin-deficient eukaryotic models is high sensitivity toward oxidative damage.[6–8]

Frataxin is a small mitochondrial protein, highly conserved, and found ubiquitously in prokaryotes and eukaryotes.[9,10] Its 3D structure has been solved for humans,[11] yeast[12] and bacterial homologs.[13] They show strong structural similarities, notably because frataxin orthologs share amino acid sequences to a high degree.[14] These similarities consist of two terminal α-helices, which form one plane over five antiparallel β-strands, which form the second plane. Moreover, another β-strand intersects the two planes to achieve an overall α–β sandwich structure.[14] A large number of the conserved acid residues (Asp, Glu) are located between the first helix and the edge of the β1-sheet. This semi-conserved acidic ridge generates a negatively charged surface, which accounts for roughly one quarter of frataxin's total accessible surface.[11] In yeast mutants, mutations of acidic residues in this region show no defects in the biosynthesis of Fe–S clusters.[15,16] However, a change in the electrostatic

[a] *Université Paris Diderot, Sorbonne Paris Cité, "Interfaces, Traitements, Organisation et Dynamique des Systèmes", CNRS-UMR 7086, 15 rue Jean Antoine de Baïf, 75205 Paris Cedex 13, France. E-mail: thanh.haduong@univ-paris-diderot.fr; Fax: +33-11-57-27-72-63; Tel: +33-11-57-27-72-39*

[b] *Université Paris Diderot, Sorbonne Paris Cité, Institut Jacques Monod, "Mitochondries, Métaux et Stress Oxydant", CNRS-UMR 7592, 15 rue Hélène Brion, 75205 Paris Cedex 13, France*

† Electronic supplementary information (ESI) available: SDS-PAGE, mass spectrometric data, Fe(III) and Fe(II) interactions with frataxin. See DOI: 10.1039/c7mt00031f

‡ Present address: Institut de Biologie de l'Ecole Normale Supérieure, 46 rue d'Ulm, 75005 Paris, France.

properties of the acidic ridge impairs this Fe–S cluster assembly, weakens the interaction between yeast frataxin (Yfh1) and the scaffold protein (Isu1), and increases oxidative damage.[17,18] In addition, mutations of these residues in bacterial frataxin lead to the loss of Fe^{2+} binding, indicating that this region can complex this cation.[13,19] Therefore, this region appears to be important to its physiological role.[20] Previous work has shown that frataxins from humans, yeast and *Escherichia coli* bind Fe^{2+} and Fe^{3+} with comparable affinities.[9,12,21] The dissociation constants of these iron–frataxin complexes are in the micromolar range, which suggests that iron interacts with frataxin with low selectivity and specificity. Moreover, mutations of the acidic residues on the α1 helix and/or β1 sheets decrease the affinity of yeast frataxin for iron without eliminating it completely.[18] Several NMR and X-ray crystallography studies show that bacterial frataxins may interact with metals other than iron, such as Co^{2+}, Eu^{3+}, Mn^{2+} and Zn^{2+}.[13,19,22]

Mitochondria require transition metals for several of their physiological functions. Iron, copper, manganese and zinc play multiple roles in protein structure and function (catalysis, electron transfer, ligand binding).[23,24] In cells, these metals form complexes with low-molecular-weight ligands to constitute labile-metal pools. More recently, liquid chromatography coupled with inductively coupled plasma mass spectrometry has shown that these complexes represent approximately 20–40% of the total mitochondrial Mn, Fe, Zn and Cu ions.[25] In this study, we investigate the *in vitro* interaction of these metal ions with yeast frataxin. We revisit the complexation of Fe^{2+} and Fe^{3+} by Yfh1 by means of emission spectroscopy, microcalorimetry and size-exclusion chromatography. We show that frataxin interacts with Cu^{+}, Cu^{2+} and Mn^{2+} with higher affinities than with iron, and establish for the first time, by the use of chemical relaxation methods, the mechanisms of iron and copper interaction with frataxin.[26,27]

Experimental

Chemical

Ferrous ammonium sulfate hexahydrate, $Fe(NH_4)_2SO_4{\cdot}6H_2O$ (Fluka), was dissolved at 10 mM in a deoxygenated 0.2 M KCl solution. FeNTA (iron nitrilotriacetic acid complex) solutions were prepared as described previously.[28] $CuSO_4$, $ZnSO_4$ and $MnCl_2$ (Prolabo) were dissolved in a 50 mM bis-Tris (2,2-bis-(hydroxymethyl)-2,2′,2″-nitrilotriethanol) and 150 mM KCl buffer. Reduced glutathione (GSH, Sigma-Aldrich) was dissolved in the same, deoxygenated, buffer. $Cu(GSH)_2$ was prepared as previously described[29] in the same buffer. Its concentration was measured before each experiment using (2,2′)-biquinoline ((2,2′)-BBQ, Fluka), which forms selectively a complex with Cu^{+}, $\varepsilon_{545} = 6370\ M^{-1}\ cm^{-1}$.[30] (2,2′)-BBQ was dissolved in acetic acid at 0.5 mg mL^{-1}.

The bis-Tris (Amresco) concentration in neutral buffers was 50 mM. The final pH values were continuously controlled and adjusted to between 6.6 and 8.6 with micro-quantities of concentrated HCl or NaOH. All final ionic strengths were adjusted to 0.2 M with KCl (Sigma-Aldrich). Except with Zn(II), Fe(III) and Cu(II), all the experiments were performed under anaerobic conditions in a glove box under argon to avoid any oxidation and reaction with oxygen to generate superoxide anions.[31]

Yfh1 mutants, growth conditions and mitochondria metal measurement

The *Saccharomyces cerevisiae* strains, and wild-type and *Δyfh1* mutants used in this study were derived from YHP499 and S150-2B as previously described.[32] Liquid cultures were grown at 30 °C in YPD media (1% yeast extract, 2% Bacto peptone, 2% D-glucose) supplemented with 200 mg L^{-1} adenine when needed. For Cu and Mn survival tests, the strains from the S150-2B background were grown to the late exponential phase, diluted in YPD, spotted onto YPD plates containing or not containing 1 mM $MnCl_2$ or 1.25 mM $CuSO_4$ and incubated for 2 days at 30 °C. Metals were measured by inductively coupled plasma atomic emission spectroscopy (Service Central d'Analyse, ISA-CNRS, Villeurbanne, France) in the mitochondria prepared from the YPH499 strains as described.[33] Zinc suppresses the iron-accumulation phenotype of *S. cerevisiae* lacking the yeast frataxin homologue (Yfh1).

Expression and purification of Yfh1

The mature full-length Yfh1 (residues 52–174) coding sequence was amplified from genomic DNA by PCR, then cloned into a pUC19 vector, and the nucleotide sequence was verified by Sanger sequencing. The *Nde*1-*Bam*H1 fragment with the coding sequence from the initiation methionine to a stop codon was subcloned into a pSBET-b bacterial vector for expression.[34] Yfh1 was then overexpressed in the *E. coli* BL21(DE3) strain (Thermo Fisher) by incubation overnight (15 h) at 37 °C with 200 rpm agitation in LBE auto-induction medium.[35] The cells were harvested by centrifugation at 4000 rpm for 15 min, and washed once with Milli-Q water. The cells were then lysed using a French press operated at 2.5 kbar in the presence of benzonase. A cell lysate of 1 : 1 (v/v) was mixed with 50 mM HEPES and 6 M urea buffer at pH 7.0 (buffer A) and kept at room temperature for 15 min. This mixture was centrifuged at 4000 rpm for 15 min at 4 °C to eliminate the insoluble proteins. The supernatant was loaded onto an anion-exchange column of DEAE-Sepharose Fast Flow (Sigma Aldrich) previously equilibrated with buffer A. The proteins were eluted by a linear gradient of NaCl from 0.1 M to 1 M. SDS-PAGE and western blot experiments using an anti-frataxin polyclonal antibody were performed to locate the fractions containing Yfh1 (Fig. S1, ESI†).[36] These were loaded onto a hydroxyapatite (BioGrad Labs) column previously equilibrated with 25 mM HEPES buffer at pH 7.0. Elution was performed with a gradient of potassium phosphate from 50 mM to 750 mM. The fractions containing Yfh1 were pooled and concentrated by Vivaspin 10000WCO (GE Healthcare Life Sciences), and then applied to a Superdex™ 200 10/300 GL size-exclusion chromatography column (Äkta purifier – GE Healthcare Life Sciences).

SDS-PAGE stained by Coomassie Brilliant Blue 1% was used to identify the fractions containing Yfh1. The isolated protein and products of in-gel digestion by trypsin were analyzed by

mass spectrometry on electrospray ionization (ESI-MS) and MALDI TOF-TOF instruments, respectively (ESI,† Fig. S2 and S3).

Protein concentrations were evaluated by the Bio Rad (Bradford) protein assay and/or spectrophotometrically (ε_{280} = 40 000 M^{-1} cm^{-1}).[37] The final solutions of frataxin were further diluted to the required concentrations in the buffers.

pH Measurements

The pH values were measured with a Jenco pH meter equipped with a Metrohm combined calomel/glass mini-electrode. The pH meter was standardized at 25 °C by the standard pH buffer values of 7.00 and 10.01 (Beckman). At the end of the measurements, the pH values were double-checked in both the buffer and the protein solutions.

Spectrofluorimetric measurements

Absorption measurements were performed at 25 °C on a Cary 4000 spectrophotometer equipped with a Peltier-thermostated cell-carrier. Fluorimetric measurements were performed at 25 °C on an Aminco-Bowman series 2 luminescence spectrometer equipped with an external thermostated water-bath for circulation. The excitation wavelength (λ_{ex}) was set at 280 nm and the emission spectra were measured between 300 and 400 nm. The spectra used for the determination of equilibrium constants were recorded at the final equilibrated state. For the anaerobic experiments, specially designed cuvettes were used and manipulated in a glove box before being transferred to the spectrometers.

The dissociation constants of the metal–frataxin complexes were determined from the spectrofluorimetric data sets collected at multiple wavelengths using the multivariate data analysis program, SPECFIT 32.[38]

Isothermal titration calorimetry

ITC measurements were performed to determine the binding affinity of $(Yfh1)_2$ for metals and the stoichiometries involved in the processes. The experiments were carried out on a TA Instruments low-volume Nano ITC with gold cells and an active cell volume of 166 μL. All the ITC titrations were performed at 25 °C with a stirring rate of 250 rpm, using a 50 μL titration syringe. Typically, an initial injection of 1 μL into the sample cell containing $(Yfh1)_2$ was followed by an automated sequence of 24 injections, each of 2 μL of the metal titrant, spaced at 5 min intervals. Control experiments, to account for the heat of dilution, were performed using a metal ion solution in the syringe and a buffer solution in the ITC cell. The data were collected automatically and were analyzed using the NanoAnalyze software (TA Instruments) and a mathematical model involving one class of independent multiple binding sites.

HPLC-size-exclusion chromatography

An HPLC system (1260 Infinity, Agilent) with a quaternary pump and absorption and emission detectors were used to identify the oligomeric species of frataxin in the presence or absence of metals. HPLC was also utilized to analyze the interaction of $Cu(GSH)_2$ with frataxin. Protein samples were prepared in 50 mM bis-Tris and 20 mM KCl, at a pH of 7.0, and loaded (20 μL) onto a size-exclusion column (Bio SEC-5, 5 μm particles, 150 Å, 7.8 mm × 300 mm) from Agilent, previously calibrated with dimeric bovine albumin (132 kDa), monomeric bovine albumin (66 kDa), ovalbumin (45 kDa), carbonic anhydrase (29 kDa), and lactalbumin (14.2 kDa). The mobile phase consisted of 50 mM KH_2PO_4 buffer at a pH of 7.0. The flow rate of the HPLC system was set at 1.0 mL min^{-1}. Elution was monitored by absorption at 280 nm and emission at 340 nm (λ_{ex} = 280 nm).

Kinetics

Stopped-flow experiments were performed on a Hi-Tech Scientific SF61DX2 stopped-flow spectrofluorimeter equipped with a Xe/Hg light source and a thermostated bath at 25 °C. Buffered aqueous solutions (50 mM bis-Tris and 150 mM KCl, μ = 0.2) of frataxin and metals were mixed using the stopped-flow device (mixing time $<$3 ms). The stopped-flow apparatus and mixing syringes were kept under pure argon in a specially designed glove box. Fluorimetric detection was used (λ_{ex} = 295 nm; $\lambda_{em} \geq$ 300 nm). All stopped-flow kinetic curves were recorded 10 times and signal-averaged.

Results

Preliminary attempts to produce recombinant Yfh1 using a classical pET21b expression vector failed, mainly because the IPTG-mediated induction of protein production was poorly efficient. The protein was purified jointly with major chaperones from *E. coli* (DnaJ, IbpA) identified by peptide mass fingerprints from SDS-PAGE-separated proteins (data not shown). We therefore cloned the open reading frame of the mature Yfh1 into the pSBET-b expression vector that carries the ArgU gene, allowing the efficient production of eukaryotic proteins in *E. coli*. The auto-induction medium described by Studier,[35] together with the two-step purification strategy, taking advantage of the low pI (4.13) of the protein, allowed us to produce up to 10 mg of purified proteins per gram of cell paste. As shown in Fig. S4 (ESI†), the protein migrated at an apparent molecular mass of ~28 kDa, while its mass measured by MALDI TOF-TOF was 13742.89 Da (corresponding to the exact computed mass of the non-modified mature protein, with a minor fraction of the protein containing the uncleaved initiation methionine residue (13873.93 Da)). In addition, Yfh1 was analyzed by high-resolution ESI mass spectrometry (Orbitrap Exactive EMR) at a low voltage[39] (Fig. S3, ESI†) and showed a molecular mass of 27499.842 Da. The size-exclusion chromatography and mass spectrometry experiments consistently indicated that the protein in the solution was recovered as a dimer.

The frataxin we obtained is the association of two identical frataxin subunits, each of which may bind metals. Therefore, our kinetic and thermodynamic analyses are based on the assumption that the two subunits have very similar behavior towards metal binding.

Thermodynamics of metal binding

The thermodynamics related to the Fe^{3+} interaction by $(Yfh1)_2$ are described in the ESI† (Fig. S5–S8).

Spectrophotometric titration of Fe(II), Cu(II), Mn(II) and Zn(II) binding to $(Yfh1)_2$. The Fe^{2+} donor to $(Yfh1)_2$ used in our experiments is ferrous ammonium sulfate in the absence or presence of reduced glutathione (Fig. 1A and Fig. S9, S10, ESI†).

The addition of Fe^{2+}, Cu^{2+}, Mn^{2+} or Zn^{2+} to a solution of $(Yfh1)_2$ leads to a decrease in fluorescence emission accompanied by a red-shift of 2–3 nm (from 334 to 336–337 nm) (Fig. 1). Since frataxin can form complexes with one or two cations,[40] we assumed that each subunit interacts in the same way. SPECFIT analysis shows that two M^{2+} complexes are produced successively with Yfh1 (eqn (1) and (2), with M = Fe, Cu, Mn or Zn):

$$Yfh1 + M^{2+} \rightleftharpoons (Yfh1)M^{II} \quad (1)$$

$$(Yfh1)M^{II} + M^{2+} \rightleftharpoons (Yfh1)M_2^{II} \quad (2)$$

with

$$K_{d1}(M^{II}) = [M^{2+}][Yfh1]/[(Yfh1)M^{II}]$$

$$K_{d2}(M^{II}) = [M^{2+}][(Yfh1)M^{II}]/[(Yfh1)M_2^{II}]$$

where $K_{d1}(Fe^{II})$ and $K_{d2}(Fe^{II})$ are measured at different pHs in the pH range of 6.5–8.5 in the presence or absence of GSH. $K_{d1}(Fe^{II})$ and $K_{d2}(Fe^{II})$ are independent of pH and GSH concentration (Table 1), with average values of $-\log K_{d1}(Fe^{II}) = 6.3 \pm 0.4$ and $-\log K_{d2}(Fe^{II}) = 4.7 \pm 0.3$.

This pH independence also occurs with Cu^{2+}, Mn^{2+} and Zn^{2+} with:

$$-\log K_{d1}(Cu^{II}) = 6.9 \pm 0.5 \text{ and } -\log K_{d2}(Cu^{II}) = 5.5 \pm 0.6.$$

$$-\log K_{d1}(Mn^{II}) = 7.4 \pm 0.1 \text{ and } -\log K_{d2}(Mn^{II}) = 6.4 \pm 0.2.$$

Table 1 Dissociation constants of $(Yfh1)Fe^{II}$ and $(Yfh1)Fe^{II}$ complexes determined by spectrophotometric titration at pH 7.0 and at 25 °C in the absence or presence of GSH

[GSH] (mM)	$-\log K_{d1}(Fe^{II})$	$-\log K_{d2}(Fe^{II})$
0	6.6 ± 0.2	4.8 ± 0.3
2.5	5.8 ± 0.1	4.5 ± 0.2
5	6.9 ± 0.6	4.7 ± 0.6
10	6.0 ± 0.2	4.8 ± 0.2

$$-\log K_{d1}(Zn^{II}) = 5.8 \pm 0.2 \text{ and } -\log K_{d2}(Zn^{II}) = 6.1 \pm 0.1.$$

Microcalorimetric titration of copper(II) binding. The affinity constants of $(Yfh1)_2$ for Cu^{2+} were also evaluated by microcalorimetry. ITC experiments showed that the binding of Cu^{2+} to $(Yfh1)_2$ is exothermic: $\Delta H_1 = -(28.2 \pm 0.5)$ kJ mol^{-1} and $\Delta H_2 = -(30 \pm 4)$ kJ mol^{-1} (Fig. 2). The data were curve-fitted by a model of multiple independent binding sites, which gave 2.2 ± 0.5 and 2.4 ± 0.3 equivalents of Cu^{2+} bound to $(Yfh1)_2$: $K_1 = (2.0 \pm 0.5) \times 10^7$ and $K_2 = (3.4 \pm 0.8) \times 10^4$. These are, within the limits of uncertainty, identical to those determined spectrophotometrically.

Copper(I) binding. The Cu^+ donor to $(Yfh1)_2$ used here is $Cu(I)GSH_2$. Its synthesis and the estimation of its Cu(I) content were performed as described elsewhere.[30,41] As shown in Fig. 3, GSH is partly oxidized during the experiment. The elution volumes are 9.5 and 10 mL for GSSG and GSH, respectively.

The HPLC chromatogram of a mixture of 1/1 equivalents of $Cu(GSH)_2$ and $(Yfh1)_2$ (Fig. 3) does not show peaks corresponding to either $Cu(GSH)_2$ (Ve = 8.8 mL) or GSH (10 mL), which excludes

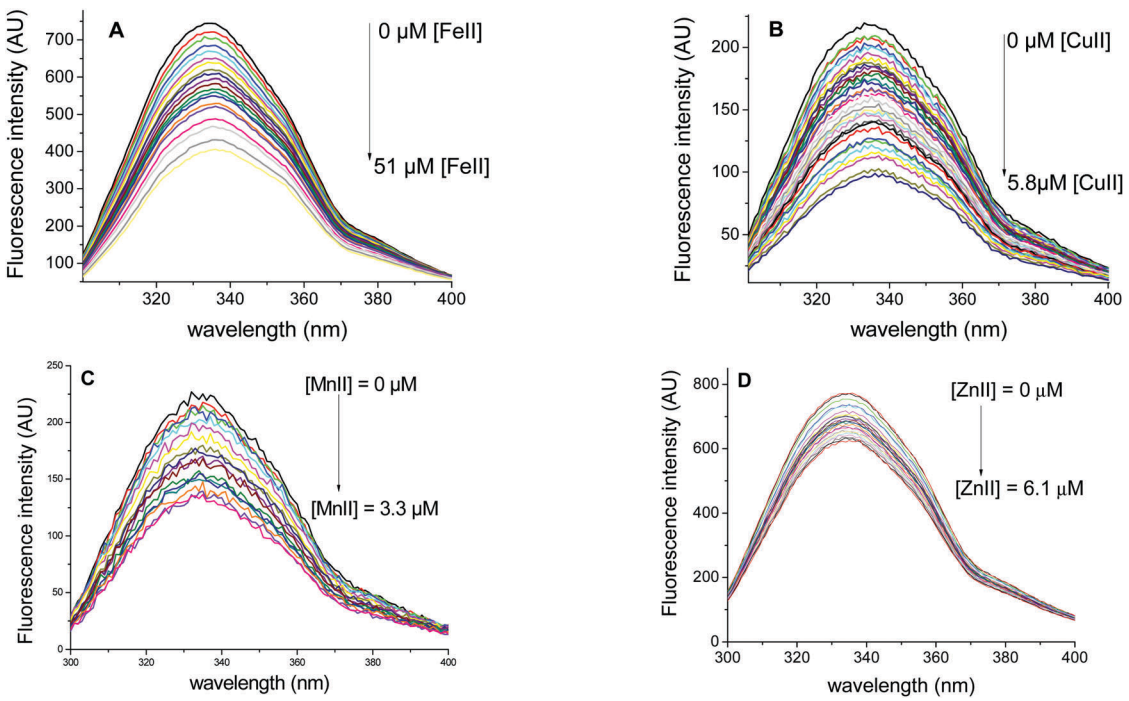

Fig. 1 Emission spectra (λ_{ex} = 280 nm) of $(Yfh1)_2$ (0.9 μM) in 50 mM bis-Tris and 150 mM KCl, pH 7.0, at different concentrations of (A) Fe^{2+} (0 μM to 51 μM), (B) Cu^{2+} (0 μM to 5.8 μM), (C) Mn^{2+} (0 μM to 3.3 μM) and (D) Zn^{2+} (0 μM to 6.1 μM) at pH 6.5.

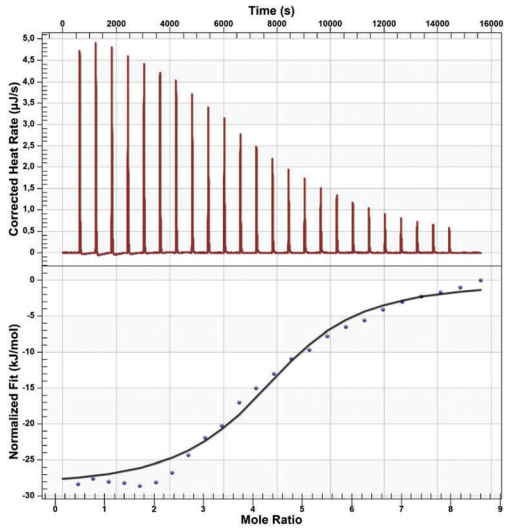

Fig. 2 Raw ITC (top) and isotherm data (bottom) for the binding of Cu^{2+} to $(Yfh1)_2$. The black lines in the bottom graph show the simulated fit to the binding isotherm data. Data were collected at 25 °C, pH 7.0, ionic strength μ = 0.2 (50 mM bis-Tris and 150 mM KCl).

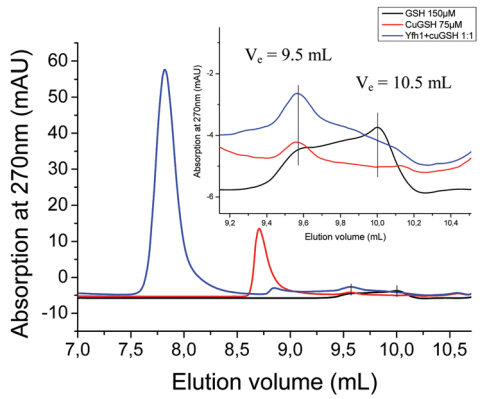

Fig. 3 Chromatograms of $Cu(GSH)_2$ of 75 µM in the absence (red) or presence of $(Yfh1)_2$ of 75 µM (blue), and of GSH of 150 µM (black). Inset: Zoom-in elution volume corresponding to GSSG/GSH at pH 7.0. Mobile phase: 50 mM KH_2PO_4 buffer, pH 7.0, elution rate 1 mL min^{-1}. Detection by UV-visible absorbance at λ = 270 nm.

Cu(I) exchange between $(Yfh1)_2$ and $Cu(GSH)_2$. Indeed, such an exchange should lead to the release of GSH into the medium. Moreover, no interaction was observed between $(Yfh1)_2$ and GSH alone (Fig. S11, ESI†). We therefore assume that we are dealing with an interaction between $Cu(GSH)_2$ and the protein.

Furthermore, under anaerobic conditions, at a pH of 7.0, the addition of $Cu(GSH)_2$ to a solution of $(Yfh1)_2$ leads to a decrease in fluorescence emission accompanied by a red-shift of 2 nm (from 334 to 336 nm) (Fig. 4A). When the fluorescence intensity is plotted against the $[Cu(GSH)_2]/[(Yfh1)_2]$ ratio, two linear sections are observed (Fig. 4B). The first line occurs for $0 \leq [Cu(GSH)_2]/[(Yfh1)_2] \leq 2$, whereas the second occurs above the ratio of 2 metal ions per $(Yfh1)_2$ with, however, a smaller slope. This implies the formation of only one complex with a stoichiometry of 2 $Cu(GSH)_2$ per $(Yfh1)_2$ (eqn (3)). Using SPECFIT analysis, the dissociation constant of the Cu^+–Yfh1 subunit complex (eqn (4)) is $-\log K_d(Cu^I) = 7.5 \pm 0.5$. The same experiments were repeated in the presence of 1.5 mM GSH at different pH values ($6.5 < pH < 7.8$). The dissociation constants were identical to those measured at pH 7.0.

$$Yfh1 + Cu(GSH)_2 \rightleftharpoons (Yfh1)Cu(GSH)_2 \quad (3)$$

with

$$K_d(Cu^I) = [Yfh1][Cu(GSH)_2]/[(Yfh1)Cu(GSH)_2] \quad (4)$$

Kinetics of metal binding

The kinetic processes related to Fe^{2+} and Fe^{3+} uptake by $(Yfh1)_2$ are described in the ESI† (Fig. S12–S16).

Copper(II). When a solution of $(Yfh1)_2$ is mixed with a solution of Cu^{2+} in bis-Tris buffer, three kinetic processes are observed (Fig. 5). The first process is fast and occurs in the 50 ms range as an exponential decrease in the fluorescence to yield a first kinetic product (Fig. 5A). The second process yields a second kinetic product, which appears as a monoexponential increase in the emission, occurring in the 200 s range (Fig. 5B). These two processes are followed by a slow kinetic phenomenon, which lasts about 2000 s (Fig. 5C). This third process seems to be independent of our experimental conditions:

$$\left(\tau_3^{Cu^{II}}\right)^{-1} = (1.2 \pm 0.3) \times 10^{-3}\ s^{-1}.$$

The reciprocal relaxation times associated with the first phenomenon of Fig. 5 depend on Cu^{2+} concentrations and pH, but are independent of Yfh1 concentrations.

Under our experimental conditions ($[Yfh1] \ll [Cu^{2+}]$) and at a given pH, there is a linear relationship between the experimental relaxation time τ^{-1} and the Cu^{2+} concentration (Fig. 6A). This can be expressed by eqn (5):

$$\left(\tau_1^{Cu^{II}}\right)^{-1} = k_{obs}\left[Cu^{2+}\right] + k_{-obs} \quad (5)$$

We ascribe this first process to the uptake of one Cu^{2+} by the Yfh1 subunit (eqn (1)).

From the slopes and intercepts of the best linear regression of τ^{-1} against $[Cu^{2+}]$ performed at seven pH values (6.0, 6.2, 6.5, 7.0, 7.3, 7.5 and 7.8), the k_{obs} and k_{-obs} values were determined (Table 2). The k_{-obs} values appear to be independent of pH, whereas k_{obs} increases with pH (Table 2). A plot of $1/k_{obs}$ against $[H^+]^n$ shows a linear relationship for n = 1 (Fig. 6B). This leads us to assume that the Cu^{2+} uptake by Yfh1 involves the transfer of a single proton. Furthermore, the Yfh1 emission spectra depend on the pH, as shown in Fig. 7. SPECFIT analysis of these spectra allows the determination of the protodissociation constant, $pK_a = 6.7 \pm 0.1$, which we ascribe to a proton loss from Yfh1 (eqn (6)). We shall therefore assume that the uptake of a first Cu^{2+} occurs by this deprotonated form of Yfh1 (eqn (6) and (7)).

$$Yfh1 \rightleftharpoons (Yfh1)' + H^+ \quad (6)$$

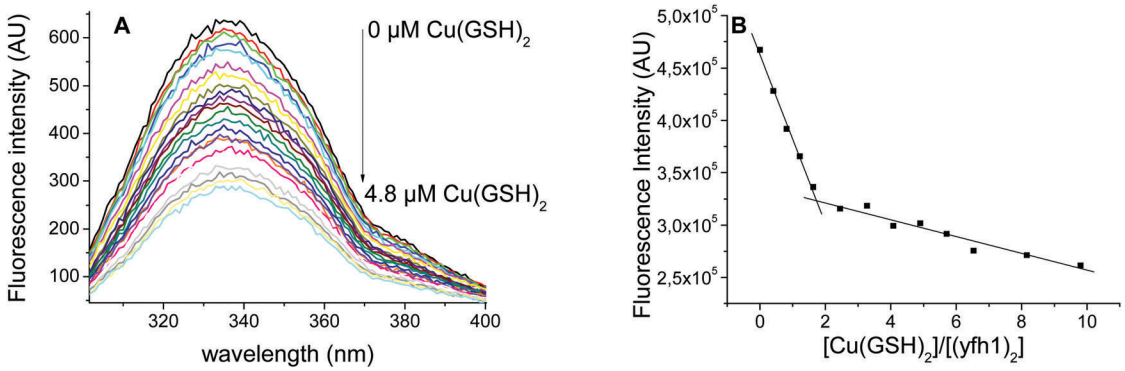

Fig. 4 (A) Emission spectra (λ_{ex} = 280 nm) of $(Yfh1)_2$ (0.24 μM) at different concentrations of $Cu(GSH)_2$ (0 μM to 4.8 μM), at pH 7.0, and ionic strength μ = 0.2 (50 mM bis-Tris and 150 mM KCl). (B) Plot of the fluorescence intensity against the $[Cu(GSH)_2]/[(Yfh1)_2]$ ratio.

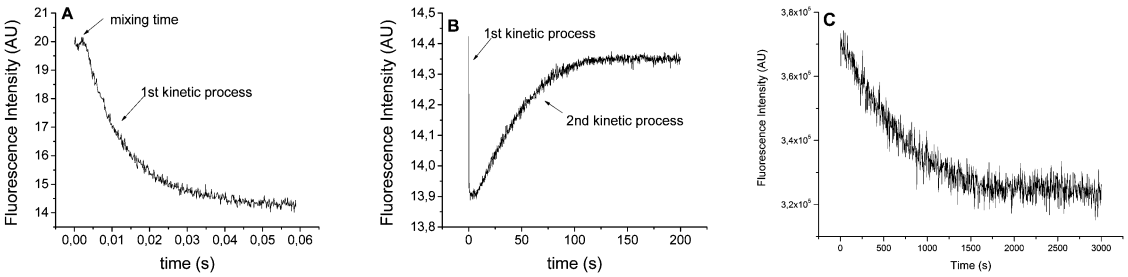

Fig. 5 Fluorescence intensity variation with time after fast mixing of a $(Yfh1)_2$ solution (0.5 μM) (A and B) with a solution of 25 μM $CuSO_4$ at pH 7.3, (C) 200 μM $CuSO_4$ at pH 7.0, 25 °C and ionic strength μ = 0.2 (50 mM bis-Tris and 150 mM KCl).

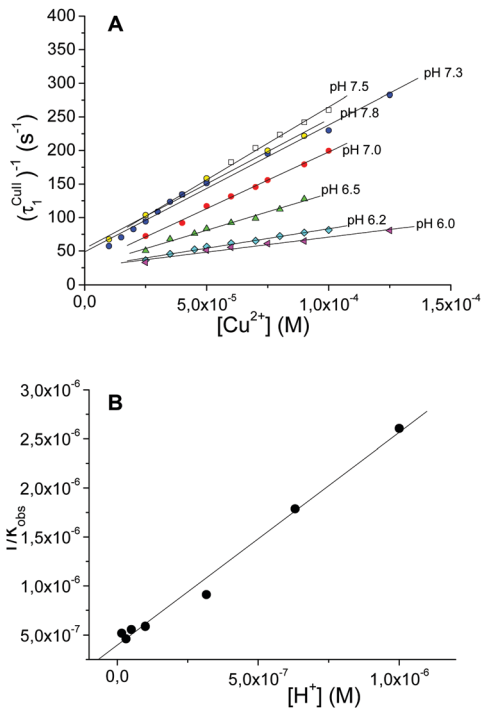

Fig. 6 (A) Plot of $\left(\tau_1^{Cu^{II}}\right)^{-1}$ against $[Cu^{2+}]$ at seven fixed pH values with $[(Yfh1)_2]$ = 0.5 μM; 25 μM ≤ $[Cu^{2+}]$ ≤ 125 μM. (B) Plot of $1/k_{obs}$ against $[H^+]$; intercept, (3.95 ± 0.4) × 10^{-7} M s; slope, 2.17 ± 0.1 s; r = 0.9947.

Table 2 Apparent rate constants k_{obs} and k_{-obs} after fast mixing of Cu^{II} and $(Yfh1)_2$ by stopped-flow

pH	k_{-obs} (s^{-1})	k_{obs} (M^{-1} s^{-1})
6.0	25.8 ± 3.1	(4.5 ± 0.4) × 10^5
6.2	27.1 ± 1.1	(5.6 ± 0.1) × 10^6
6.5	26.2 ± 3.0	(1.1 ± 0.05) × 10^6
7.0	28.7 ± 2.8	(1.7 ± 0.04) × 10^6
7.3	34.4 ± 3.9	(1.8 ± 0.07) × 10^6
7.5	47.6 ± 3.6	(2.2 ± 0.05) × 10^6
7.8	52.7 ± 4.3	(1.9 ± 0.07) × 10^6

$$(Yfh1)' + Cu^{2+} \underset{k_{-1}^{Cu^{II}}}{\overset{k_1^{Cu^{II}}}{\rightleftharpoons}} (Yfh1)Cu^{II} \qquad (7)$$

with

$$K_a = [(Yfh1)'][H^+]/[(Yfh1)]$$

and

$$K_1^{Cu^{II}} = k_1^{Cu^{II}} \Big/ k_{-1}^{Cu^{II}} = \left[(Yfh1)Cu^{II}\right] \Big/ \left[(Yfh1)'\right]\left[Cu^{2+}\right].$$

The reciprocal relaxation time associated with eqn (7) can be expressed as eqn (8) (ESI†):

$$\left(\tau_1^{Cu^{II}}\right)^{-1} = k_1^{Cu^{II}}\left(1 + \frac{[H^+]}{K_a}\right)^{-1} \times \left[Cu^{2+}\right] + k_{-1}^{Cu^{II}} \qquad (8)$$

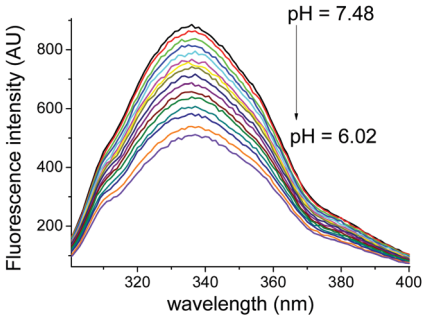

Fig. 7 Emission spectra (λ_{ex} = 280 nm) of $(Yfh1)_2$ (0.12 μM) at different pH values, at ionic strength μ = 0.2, 25 °C (50 mM bis-Tris and 150 mM KCl).

with

$$k_{obs} = k_1^{Cu^{II}}\left(1 + \frac{[H^+]}{K_a}\right)^{-1}.$$

From the slope and intercept of the best lines of Fig. 6B, $k_1^{Cu^{II}} = (2.5 \pm 0.2) \times 10^6\ M^{-1}\ s^{-1}$ and $K_a = (1.8 \pm 0.3) \times 10^{-7}$ M. K_a is, within the limits of uncertainty, identical to that determined by spectrophotofluorimetry (Fig. 7).

Upon knowing K_a, a good linear regression of all the experimental data at different pH values and $[Cu^{2+}]$ against eqn (8) is obtained (Fig. 8). $k_1^{Cu^{II}} = (2.7 \pm 0.1) \times 10^6\ M^{-1}\ s^{-1}$ is confirmed within the experimental uncertainty, and $k_{-1}^{Cu^{II}} = 30.4 \pm 2.1\ s^{-1}$ is determined from the intercept of the best regression line of Fig. 8. This allows the measurement of $K_1^{Cu^{II}} = k_1^{Cu^{II}} / k_{-1}^{Cu^{II}} = 8.9 \times 10^4\ M^{-1}$.

The experimental reciprocal relaxation times related to the second phenomenon of Fig. 5 depend on the Cu^{2+} concentration and $[H^+]$. This process cannot describe a pure acid–base reaction. Indeed, proton transfers are diffusion-controlled and therefore occur in the micro-second to tens of micro-seconds range.[42,43] The only model that concurs with our experimental observations implies that the uptake of the second Cu^{2+} is rate-limited by a conformational change that controls a proton-transfer reaction (eqn (9) and (10)):[44,45]

$$(Yfh1)Cu^{II} + Cu^{2+} \rightleftharpoons ((Yfh1)Cu_2^{II})' \quad (9)$$

$$((Yfh1)Cu_2^{II})' \underset{k_{-2}^{Cu^{II}}}{\overset{k_2^{Cu^{II}}}{\rightleftharpoons}} (Yfh1)Cu_2^{II} + H^+ \quad (10)$$

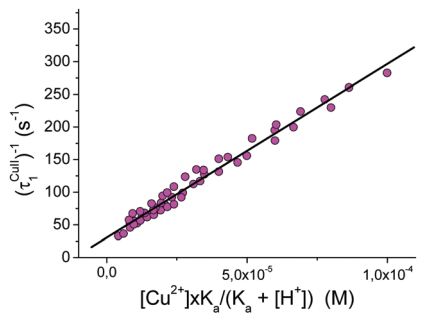

Fig. 8 Plot of $\left(\tau_1^{Cu^{II}}\right)^{-1}$ against $[Cu^{2+}] \times K_a/(K_a + [H^+])$; intercept of 30.4 ± 2.1 s^{-1}; slope (2.7 ± 0.05) × 10^6 M^{-1} s^{-1}; r = 0.98934.

The reciprocal relaxation time associated with rate-limiting eqn (10) is expressed as eqn (11) (ESI†):

$$\frac{\left(\tau_2^{Cu^{II}}\right)^{-1}}{[H^+]} = k_2^{Cu^{II}} \frac{[Cu^{2+}]}{[H^+]\left(K_{d1}K_{d2} + K_{d2}[Cu^{2+}] + [Cu^{2+}]^2\right)} + k_{-2}^{Cu^{II}} \quad (11)$$

with K_{d1} (=1/K_1) and K_{d2} (=1/K_2) as determined by the ITC.

The plot of the data related to eqn (11) is linear (Fig. 9). From the slope of the best line, $k_{-2}^{Cu^{II}} = 0.141 \pm 0.003\ M^{-1}\ s^{-1}$ is determined.

This third process of Fig. 5 is independent of our experimental parameters. It is, therefore, assumed to be a first-order rate process that can be ascribed to a monomolecular reaction, such as a change in conformation:[44]

$$\left(\tau_3^{Cu^{II}}\right)^{-1} = (1.4 \pm 0.5) \times 10^{-3}\ s^{-1}$$

Copper(I). When a solution of $(Yfh1)_2$ is mixed with a solution of $Cu(GSH)_2$ in bis-Tris buffer, three kinetic processes are observed (Fig. 10). The first appears as a monoexponential increase in the fluorescence intensity occurring in the 500 ms range (Fig. 10A). The second process takes place in the 20 s range as a monoexponential increase in the emission (Fig. 10B). Finally, the last process is slow, lasting about 3000 s (Fig. 10C).

The experimental reciprocal relaxation times related to this first process (Fig. 10A) depend on the $Cu(GSH)_2$ concentrations. They increase linearly with $[Cu(GSH)_2]$ to reach a plateau above 75 μM (Fig. 11). We assume that this phenomenon is the uptake of a first Cu^+ followed by a monomolecular reaction, such as a conformational change (eqn (12) and (13)) (ESI†).

$$(Yfh1) + Cu^+ \rightleftharpoons \{(Yfh1)Cu^I\} \quad (12)$$

$$\{(Yfh1)Cu^I\} \underset{k_{-1}^{Cu^I}}{\overset{k_1^{Cu^I}}{\rightleftharpoons}} (Yfh1)Cu^I \quad (13)$$

with overall dissociation constants

$$K_1^{Cu^I} = \frac{[(Yfh1)Cu^I]}{[Yfh1][Cu^I]}$$

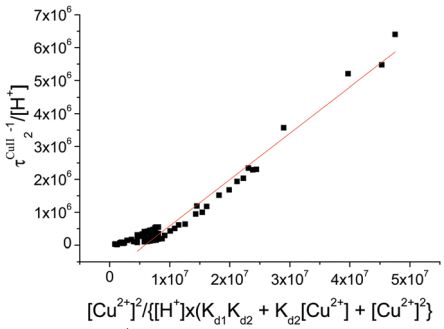

Fig. 9 Plot of $\left(\tau_2^{Cu^{II}}\right)^{-1} / [H^+]$ against $[Cu^{2+}]^2/\{[H^+] \times (K_{d1} \times K_{d2} + K_{d2} \times [Cu^{2+}] + [Cu^{2+}]^2)\}$; the best regression line gave an intercept of (−8.2 ± 0.6) × 10^5 s^{-1}, slope 0.141 ± 0.003 M^{-1} s^{-1}, r = 0.97763.

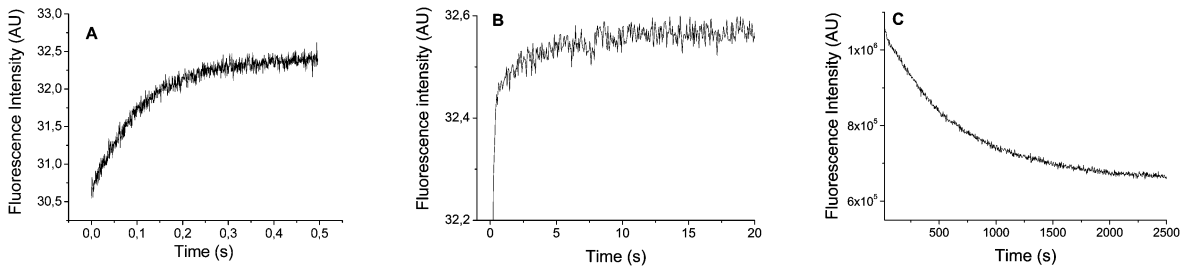

Fig. 10 Fluorescence intensity variation with time after fast mixing of a $(Yfh1)_2$ solution (1 μM) with a solution of 20 μM $Cu(GSH)_2$ at pH 7.0, 25 °C, and ionic strength μ = 0.2 (50 mM bis-Tris and 150 mM KCl). (A) Recorded over 500 ms, (B) recorded over 20 s, and (C) recorded over 2500 s.

and

$$\left(K_1^{Cu^I}\right)' = \frac{[(Yfh1)Cu^I]}{[\{(Yfh1)Cu^I\}]} = \frac{k_1^{Cu^I}}{k_{-1}^{Cu^I}}$$

The reciprocal relaxation time equation associated with eqn (13) can be expressed as eqn (14):

$$\left(\tau_1^{Cu^I}\right)^{-1} = \frac{k_1^{Cu^I}[Cu^+]}{[Cu^+] + K_1^{Cu^I}} + k_{-1}^{Cu^I} \qquad (14)$$

Varying $K_1^{Cu^I}$ from 1 to 100 μM with a $\Delta K_1^{Cu^I}$ step of 5 μM shows that the best linear regression of $\left(\tau_1^{Cu^I}\right)^{-1}$ against $[Cu^+]\Big/\left(K_1^{Cu^I} + [Cu^+]\right)$ is obtained for $K_1^{Cu^I} = 35 \pm 5$ μM (Fig. 11B). From the slope and intercept of the best line, $k_1^{Cu^I} = 10.8 \pm 0.8\ s^{-1}$, $k_{-1}^{Cu^I} = 5.8 \pm 0.5\ s^{-1}$ and $\left(K_1^{Cu^I}\right)' = 1.9 \pm 0.3$.

The second and third processes (Fig. 10B and C) are independent of $Cu(GSH)_2$ concentrations. They are therefore assumed to be monomolecular reactions, which may imply conformational changes:[46]

$$\left(\tau_2^{Cu^I}\right)^{-1} = (2.8 \pm 0.3) \times 10^{-1}\ s^{-1}$$

and

$$\left(\tau_3^{Cu^I}\right)^{-1} = (1.6 \pm 0.7) \times 10^{-3}\ s^{-1}$$

We evaluated the effect of frataxin deficiency *in vivo* in yeast, in relation to copper homeostasis. As shown in Fig. 12, there was marked growth inhibition of a frataxin deficient strain (*Δyfh1*) assayed on a rich solid medium supplemented with 1.25 mM copper. A similar inhibition of growth was observed when the *Δyfh1* cells were plated on manganese (1 mM) containing medium. The metal content varied significantly in purified mitochondria from wild-type (WT) or *Δyfh1* cells grown under standard conditions (YPD liquid medium). As previously shown, iron accumulated in frataxin-deficient mitochondria (272 ± 10.97 *vs.* 110 ± 6.93 μg g^{-1} mitochondria). We also found an increased amount of copper in the frataxin-deficient mitochondria compared to the WT condition (13.6 ± 0.87 *vs.* 9.4 ± 0.46 μg g^{-1} mitochondria).

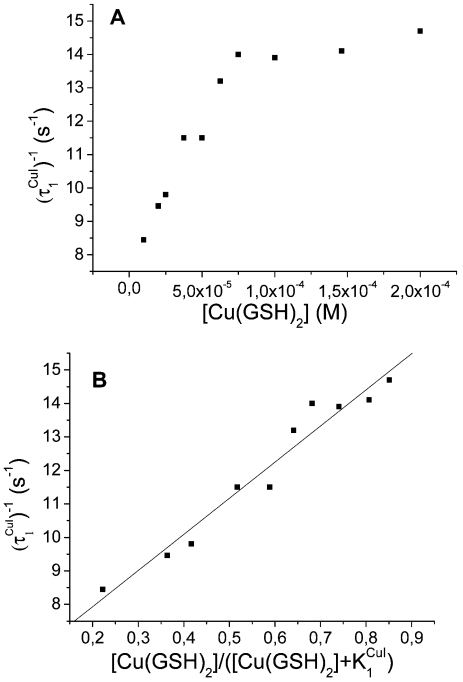

Fig. 11 (A) Plot of $\left(\tau_1^{Cu^I}\right)^{-1}$ against $[Cu(GSH)_2]$ at pH 7.0 and 25 °C. (B) Plot of $\left(\tau_1^{Cu^I}\right)^{-1}$ against $[Cu(GSH)_2]\Big/\left([Cu(GSH)_2] + K_1^{Cu^I}\right)$ with $K_1^{Cu^I} = 35$ μM; slope, 10.8 ± 0.8 s^{-1}; intercept, 5.8 ± 0.5 s^{-1}; r = 0.98418.

Discussion

Oligomeric form of yeast frataxin

In this work, we expressed, extracted and purified yeast frataxin as a dimer, as established by mass spectrometry and size-exclusion chromatography. Although the frataxin obtained from a psychrophilic bacterium is mainly monomeric, a dimeric fraction exists at high concentrations.[22] In addition, *in vitro* in the absence of iron, Yfh1 was found to be homo-oligomerized 2 weeks after its isolation.[40] To the best of our knowledge, in the absence of a metal, oligomerization does not occur *in vivo*.

Metal–Yfh1 interaction

Frataxin has an acidic ridge that accounts for almost a quarter of its surface. This area seems to be essential for its physiological function. The exposed acidic residues of Yfh1 are located on the

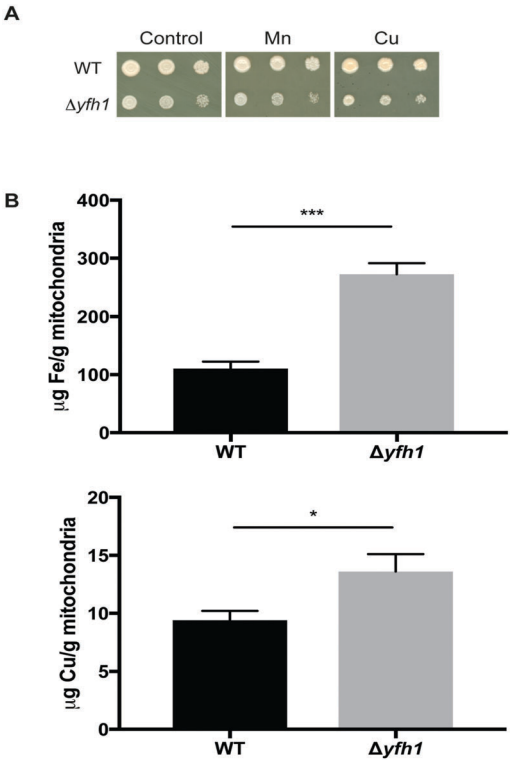

Fig. 12 Frataxin yeast mutant sensitivity to Mn and Cu and the mitochondrial metal measurement. (A) Sensitivity of the wild-type and *Δyfh1* mutant strains to 1 mM Mn and 1.25 mM Cu. (B) Fe and Cu contents measured by ICP-AES. Data represent means ± SEM (n = 3). Statistical analysis: unpaired T-test, ***, p = 0.0002; *, p = 0.0129.

α1 helix and the β1 strand, and are semi-conserved between the different species (D78, D86, E89, E90, and D101). The aim of this work was to further investigate the specificity of iron binding to frataxin. We report here the thermodynamic parameters for the formation of a mitochondrial metal complex with yeast frataxin as determined by microcalorimetry, emission spectrophotometry and size-exclusion chromatography, along with the kinetics of the interactions of Yfh1 with Fe(II), Fe(III), Cu(I) and Cu(II). The bioavailable metal pools in mitochondria contain mainly iron, zinc, copper and manganese.[23,25] These metals are weakly complexed by low-molecular-weight ligands. In yeast mitochondria, the major Fe complex and the dominant copper species are at concentrations of ~90 μM and ~16 μM, respectively.[25] On the other hand, the concentration of yeast frataxin in the mitochondria was estimated to be in the μM range (0.4 to 60 μM).[47]

We confirmed by fluorescence that yeast frataxin can bind Fe(II), with dissociation constants of 5.0×10^{-7} M for the $(Yfh1)Fe^{II}$ complex and 2.0×10^{-5} M for the second $(Yfh1)Fe_2^{II}$ complex. The average dissociation constant for the 1/1 iron/frataxin complex is 10 μM, which is close to the K_d values previously determined for Yfh1 by Cook *et al.* (3 and 2 μM) and for CyaY by Bou-Abdallah *et al.* (~4 μM).[21,40] This is in line with our hypothesis about the similar behavior in the dimer of each of the frataxin subunits towards complex formation. This, however, does not imply that the folding of each subunit is identical to that of the free monomer. We also determined the affinity constants of yeast frataxin for Mn^{2+} and Zn^{2+} (Table 3). Manganese binds Yfh1 tighter than iron, whereas the first Yfh1–Zn complex is weaker. Previous studies have shown that manganese can perturb the NMR spectra of bacterial frataxin (CyaY), and manganese supplementation in a culture of Yfh1-deficient cells (*Δyfh1*) restores the enzymatic activities of some iron–sulfur proteins.[19,48] We therefore assumed that frataxin may be involved in manganese homeostasis and, for the first time, determined *in vitro* the affinity constants of manganese for Yfh1.

We showed that frataxin also binds copper. Indeed, Seguin *et al.* reported that copper added to the growth medium is more toxic for *Δyfh1* cells than for wild-type cells,[49] as confirmed in the present study. Previous studies reported a lack of manganese in *Δyfh1* cells.[48] However, we found some toxicity of manganese *in vivo* in the *Δyfh1* context. The mitochondrial metal context was affected in the *Δyfh1* cells, where both iron and copper concentrations were increased compared to the WT cells. In addition, copper disregulation is observed in the dentate nucleus of FA patients, where iron overload does not occur. In this organelle, the net amounts of Fe, Cu and Zn are constant, whereas their distribution is altered. The Cu- and Zn-rich regions broaden and overlap extensively with the Fe-rich region. The atrophy of the dentate nucleus of FA correlates with Cu and Zn redistribution rather than with Fe overload.[50] A recent study showed that in a *Drosophila* model of FA disease, the amounts of metals other than iron are increased. It was therefore suggested that copper and zinc chelation and alteration of the expression of genes involved in the transport of these metals can restore several phenotypes of the FA fly model.[51] We showed here that $(Yfh1)_2$ interacts not only with Cu(II) but also with Cu(I), with higher affinities than Fe(II) (Table 3). The formation of complexes between Cu(II) and $(Yfh1)_2$ is enthalpy-favored ($\Delta H < 0$, Fig. 2). This indicates coordination and/or electrostatic interactions between Cu(II) and protein residues. As in the case of Fe(II), Yfh1 presents two independent binding sites for Cu(II). The affinity constants involved in the first complex, (Yfh1)M, and in the second one, $(Yfh1)M_2$, are higher for Cu(II) than for Fe(II), but the highest affinity is that for the complex formed between the Yfh1 subunit and one $Cu(GSH)_2$ ($\sim 10^{7.5}$ M^{-1}). Copper is essential for the activity of respiratory, metabolic and stress-response enzymes. Redox cycling between Cu(II) and Cu(I) oxidation states is a fundamental requirement for single-electron transfer reactions in copper-containing proteins. In mitochondria, copper is

Table 3 Comparison of dissociation constants of metal–Yfh1 complexes determined by spectrophotometric titration at pH 7.0 and at 25 °C

Fe^{II}		Cu^{II}		$Cu(GSH)_2$	Mn^{II}		Zn^{II}	
$-\log K_{d1}$	$-\log K_{d2}$	$-\log K_{d1}$	$-\log K_{d2}$	$-\log K_d$	$-\log K_{d1}$	$-\log K_{d2}$	$-\log K_{d1}$	$-\log K_{d2}$
6.6 ± 0.2	4.8 ± 0.3	6.9 ± 0.3	5.5 ± 0.3	7.5 ± 0.3	7.4 ± 0.1	6.4 ± 0.2	5.8 ± 0.2	6.1 ± 0.1

required for the function of two copper enzymes, cytochrome *c* oxidase, the last electron acceptor in the respiratory chain, and superoxide dismutase 1, a copper–zinc enzyme involved in oxidative stress.[36] This protein is mainly cytosolic; nevertheless, about 5% is localized in the mitochondrial intermembane space.[52] In a Fenton-like reaction, Cu(I) generates reactive oxygen species, which can damage cell components. To avoid radical formation, copper transfer occurs *via* a direct protein–protein interaction between copper enzymes and copper chaperones.[53,54] These proteins present an α–β sandwich structure similar to that found in frataxin. On the other hand, frataxin does not possess the conserved CXXC motif involved in Cu(I) binding to copper chaperones. Nevertheless, in addition to the negatively charged residues at the surface of Yfh1, there are three histidines (H74, H83 and H95) and a cysteine (C98), which are well known to be Cu(II) and Cu(I) ligands, and which may thus improve complex formation between these metals and frataxin.

Role of glutathione

The Cu(I) used in our experiment is in the form of the $Cu^{I}(GSH)_2$ complex. Reduced glutathione is the most abundant non-protein thiol molecule in cells. It contributes to thiol redox control and plays a role in iron metabolism in the cytoplasm and mitochondria.[55–57] The mitochondrial concentration of GSH varies from 10 to 14 mM.[58] Thus, it may form a stable complex with labile Cu(I).[59] We showed by size-exclusion chromatography that $(Yfh1)_2$ interacts with the entire $Cu(GSH)_2$ complex, but not with GSH (Fig. S12, ESI†). Furthermore, the presence of GSH in the medium has no effect on the dissociation constants of the Cu(I)- and Fe(II)–frataxin complexes (Table 1). In the cytoplasm, Fe(II)–GSH is the dominant constituent of the labile-iron pool and provides iron to the mitochondria for heme and iron–sulfur cluster maturation.[60] In addition, in Yfh1-depleted cells, iron accumulates in the mitochondria, leading to an increase in GSH import or a decrease in its export.[61] Glutathione can coordinate and stabilize $[Fe_2S_2]$ iron–sulfur centers.[62] However, in glutaredoxin, GSH ligands are unstable and can be exchanged with free GSH, which inhibits Fe–S cluster transfer to ferredoxin.[63] Frataxin is involved in Fe–S cluster (ISC) biosynthesis. It interacts with the Fe–S cluster machinery composed of the cysteine desulfurase NfS1, its activator Isd11 and the scaffold protein Isu1. Nevertheless, the role of Yfh1 in Fe–S cluster biosynthesis is still unclear. As frataxin is presumably an iron-binding protein and as it interacts with Isu1, it was first thought to provide iron to the Fe–S cluster.[64] Yoon *et al.* showed that a single mutation (M107I) in Isu1 improves the Fe–S cluster enzymatic activity in Yfh1-depleted cells, implying that frataxin plays a minor role as an iron donor.[65,66] Recently, frataxin was suggested to be an allosteric effector of the ISC complex: the bacterial ortholog of frataxin, CyaY, strengthens the interaction between desulfurase and scaffold proteins in bacteria.[67] Furthermore, Yfh1 stimulates the binding of cysteine to Nfs1 by inducing the exposure of the substrate-binding site, which enhances its activity.[68,69] Moreover, human frataxin increases the rate of persulfide formation on human scaffold protein (IscU) and of sulfur transfer from Nfs1 persulfide to IscU or to small thiols, such as cysteine or glutathione.[70] We have shown here that yeast frataxin has a higher affinity for $Cu(GSH)_2$ than for the other mitochondrial metals, whereas it cannot bind GSH (ESI†). The role of this Yfh1–($Cu(GSH)_2$) complex is still not fully understood.

Kinetics of metal-uptake by yeast frataxin

We report here the mechanisms of metal-uptake by yeast frataxin (Table 4). For all the metals studied, we observed at least three kinetic steps. The first step always corresponds to the uptake of a first cation. It is fast and occurs in the 50 to 500 ms range. With Fe(II) and Cu(I), the reciprocal relaxation times related to these first kinetic steps increase with the concentration of metal to attain a plateau (Fig. 11A and Fig. S14, ESI†). As already described, this implies a fast cation uptake followed by a monomolecular reaction, such as a conformational change (Table 4).[44,71,72] The equilibrium constants related to these conformational changes are identical for the two metals. These first processes are followed by two other kinetic steps. In the case of Fe(II), the

Table 4 Metal uptake by Yfh1

Reaction		Direct rate constant	Reverse rate constant	Equilibrium constant
Fe^{II} uptake				
$Yfh1 + Fe^{2+} \rightleftharpoons \{(Yfh1)Fe^{II}\}$	(S1)			$(5.0 \pm 0.1) \times 10^3\ M^{-1}$
$\{(Yfh1)Fe^{II}\} \rightleftharpoons (Yfh1)Fe^{II}$	(S2)	$23 \pm 1\ s^{-1}$	$11.5 \pm 0.7\ s^{-1}$	2.0 ± 0.1
$(Yfh1)Fe^{II} + Fe^{2+} \rightleftharpoons (Yfh1)Fe^{II}_2$	(S9)	$(1.15 \pm 0.04) \times 10^3\ M^{-1}\ s^{-1}$	$(9.9 \pm 1.3) \times 10^{-2}\ s^{-1}$	$(1.2 \pm 0.2) \times 10^4\ M^{-1}$
Fe^{III} uptake				
$Yfh1 + Fe^{3+} \rightleftharpoons (Yfh1)Fe^{III}$	(S31)	$(11.5 \pm 0.5) \times 10^4\ M^{-1}\ s^{-1}$	$3.4 \pm 0.7\ s^{-1}$	$(3.4 \pm 0.8) \times 10^4\ M^{-1}$
Cu^{II} uptake				
$Yfh1 \rightleftharpoons (Yfh1)' + H^+$	(6)			$(1.8 \pm 0.3) \times 10^{-7}$ M
$(Yfh1)' + Cu^{2+} \rightleftharpoons (Yfh1)Cu^{II}$	(7)	$(2.7 \pm 0.1) \times 10^6\ M^{-1}\ s^{-1}$	$30.4 \pm 2.1\ s^{-1}$	$(8.9 \pm 0.9) \times 10^4\ M^{-1}$
$(Yfh1)Cu^{II} + Cu^{2+} \rightleftharpoons ((Yfh1)Cu^{II}_2)'$	(8)			
$((Yfh1)Cu^{II}_2)' \rightleftharpoons (Yfh1)Cu^{II}_2 + H^+$	(9)		$0.141 \pm 0.003\ M^{-1}\ s^{-1}$	
$Cu(GSH)_2$ uptake				
$Yfh1 + Cu^{+} \rightleftharpoons \{(Yfh1)Cu^{I}\}$	(12)			$(2.9 \pm 0.4) \times 10^4\ M^{-1}$
$\{(Yfh1)Cu^{I}\} \rightleftharpoons (Yfh1)Cu^{I}$	(13)	$10.8 \pm 0.8\ s^{-1}$	$5.8 \pm 0.5\ s^{-1}$	1.9 ± 0.3

second step is the uptake of a second iron and the third step is a conformational change which can stabilize the iron–Yfh1 complex. As Yfh1 can complex only one $Cu(GSH)_2$, the second and third kinetic phenomena are monomolecular reactions.

On the other hand, the first Cu(II) is acquired from the deprotonated form of Yfh1 in the 20 ms range. The pK_a value of this proton-transfer reaction is 6.7 ± 0.1 (Table 4), which may imply deprotonation of a histidine residue. Indeed, on the acidic surface of the protein, H74, H83 and H95 may be involved in interactions with Cu(II). This phenomenon is followed by a second kinetic process, which corresponds to the uptake of a second Cu(II). A third slow kinetic phenomenon lasts about 3000 s leading to thermodynamic equilibrium.

For Fe(III), the first phenomenon is the uptake of a first cation (see ESI†). Although an oligomer of frataxin is formed in the presence of 9 atoms of Fe(III), the second and third kinetic processes are independent of our experimental parameters. These are assumed to be changes in the conformation allowing the uptake of another Fe(III) or oligomerization.

Conclusions

This work revisited the formation of complexes between iron and frataxin, and the proposed mechanisms for these interactions. In addition, we investigated the mitochondrial metal–frataxin interaction and confirmed that the affinity of frataxin for Fe^{2+} is lower than for the metals studied. The best affinity constant was found to be for Mn^{2+} and $Cu(GSH)_2$. The role of the (Yfh1)–$Cu(GSH)_2$ complex is unknown, and further experiments are required to determine its possible involvement in Fe–S cluster biosynthesis or in protection against oxidative stress.

Acknowledgements

The authors thank Dr J. S. Lomas for carefully reading the manuscript. This work was supported by the CNRS, by the University Paris Diderot (Paris, France) and by a PhD grant to THLH from the University of Science and Technology of Hanoi.

Notes and references

1 A. Abrahao, J. L. Pedroso, P. Braga-Neto, E. Bor-Seng-Shu, P. de Carvalho Aguiar and O. G. Barsottini, Milestones in Friedreich ataxia: more than a century and still learning, *Neurogenetics*, 2015, **16**, 151–160.

2 A. Bayot, R. Santos, J. M. Camadro and P. Rustin, Friedreich's ataxia: the vicious circle hypothesis revisited, *BMC Med.*, 2011, **9**, 112.

3 M. V. Busi and D. F. Gomez-Casati, Exploring frataxin function, *IUBMB Life*, 2012, **64**, 56–63.

4 R. A. Vaubel and G. Isaya, Iron–sulfur cluster synthesis, iron homeostasis and oxidative stress in Friedreich ataxia, *Mol. Cell. Neurosci.*, 2013, **55**, 50–61.

5 T. Yoon and J. A. Cowan, Frataxin-mediated iron delivery to ferrochelatase in the final step of heme biosynthesis, *J. Biol. Chem.*, 2004, **279**, 25943–25946.

6 J. H. Kim, M. Sedlak, Q. Gao, C. P. Riley, F. E. Regnier and J. Adamec, Oxidative stress studies in yeast with a frataxin mutant: a proteomics perspective, *J. Proteome Res.*, 2009, **9**, 730–736.

7 E. Napoli, F. Taroni and G. A. Cortopassi, Frataxin, Iron–Sulfur Clusters, Heme, ROS, and Aging, *Antioxid. Redox Signaling*, 2006, **8**, 506–516.

8 H. Seznec, D. Simon, C. Bouton, L. Reutenauer, A. Hertzog, P. Golik, V. Procaccio, M. Patel, J. C. Drapier, M. Koenig and H. Puccio, Friedreich ataxia: the oxidative stress paradox, *Hum. Mol. Genet.*, 2005, **14**, 463–474.

9 S. Adinolfi, M. Trifuoggi, A. S. Politou, S. Martin and A. Pastore, A structural approach to understanding the iron-binding properties of phylogenetically different frataxins, *Hum. Mol. Genet.*, 2002, **11**, 1865–1877.

10 T. J. Gibson, E. V. Koonin, G. Musco, A. Pastore and P. Bork, Friedreich's ataxia protein: phylogenetic evidence for mitochondrial dysfunction, *Trends Neurosci.*, 1996, **19**, 465–468.

11 S. Dhe-Paganon, R. Shigeta, Y. I. Chi, M. Ristow and S. E. Shoelson, Crystal structure of human frataxin, *J. Biol. Chem.*, 2000, **275**, 30753–30756.

12 Y. He, S. L. Alam, S. V. Proteasa, Y. Zhang, E. Lesuisse, A. Dancis and T. L. Stemmler, Yeast Frataxin Solution Structure, Iron Binding, and Ferrochelatase Interaction, *Biochemistry*, 2004, **43**, 16254–16262.

13 M. Nair, S. Adinolfi, C. Pastore, G. Kelly, P. Temussi and A. Pastore, Solution structure of the bacterial frataxin ortholog, CyaY: mapping the iron binding sites, *Structure*, 2004, **12**, 2037–2048.

14 K. Z. Bencze, K. C. Kondapalli, J. D. Cook, S. McMahon, C. Millan-Pacheco, N. Pastor and T. L. Stemmler, The structure and function of frataxin, *Crit. Rev. Biochem. Mol. Biol.*, 2006, **41**, 269–291.

15 K. Aloria, B. Schilke, A. Andrew and E. A. Craig, Iron-induced oligomerization of yeast frataxin homologue Yfh1 is dispensable *in vivo*, *EMBO Rep.*, 2004, **5**, 1096–1101.

16 O. Gakh, S. Park, G. Liu, L. Macomber, J. A. Imlay, G. C. Ferreira and G. Isaya, Mitochondrial iron detoxification is a primary function of frataxin that limits oxidative damage and preserves cell longevity, *Hum. Mol. Genet.*, 2006, **15**, 467–479.

17 A. R. Correia, T. Wang, E. A. Craig and C. M. Gomes, Iron-binding activity in yeast frataxin entails a trade off with stability in the alpha1/beta1 acidic ridge region, *Biochem. J.*, 2010, **426**, 197–203.

18 F. Foury, A. Pastore and M. Trincal, Acidic residues of yeast frataxin have an essential role in Fe–S cluster assembly, *EMBO Rep.*, 2007, **8**, 194–199.

19 C. Pastore, M. Franzese, F. Sica, P. Temussi and A. Pastore, Understanding the binding properties of an unusual metal-binding protein–a study of bacterial frataxin, *FEBS J.*, 2007, **274**, 4199–4210.

20 J. Huang, E. Dizin and J. A. Cowan, Mapping iron binding sites on human frataxin: implications for cluster assembly

on the ISU Fe–S cluster scaffold protein, *J. Biol. Inorg. Chem.*, 2008, **13**, 825–836.
21 F. Bou-Abdallah, S. Adinolfi, A. Pastore, T. M. Laue and N. Dennis Chasteen, Iron binding and oxidation kinetics in frataxin CyaY of *Escherichia coli*, *J. Mol. Biol.*, 2004, **341**, 605–615.
22 M. E. Noguera, E. A. Roman, J. B. Rigal, A. Cousido-Siah, A. Mitschler, A. Podjarny and J. Santos, Structural characterization of metal binding to a cold-adapted frataxin, *J. Biol. Inorg. Chem.*, 2015, **20**, 653–664.
23 A. Atkinson and D. R. Winge, Metal acquisition and availability in the mitochondria, *Chem. Rev.*, 2009, **109**, 4708–4721.
24 F. Pierrel, P. A. Cobine and D. R. Winge, Metal Ion availability in mitochondria, *BioMetals*, 2007, **20**, 675–682.
25 S. P. McCormick, M. J. Moore and P. A. Lindahl, Detection of labile Low-Molecular mass Transition Metal Complexes in Mitochondria, *Biochemistry*, 2015, **54**, 3442–3453.
26 C. F. Bernasconi, *Relaxation kinetics*, Academic Press, New-York, 1976.
27 M. Eigen and L. DeMaeyer, in *Relaxation methods*, ed. S. L. Friess, E. S. Lewis and A. Weissberger, Techniques of organic chemistry – Investigation of rates and mechanism of reactions, part II, Wiley Intersciences, New York, 1963, pp. 895–1029.
28 J. M. El Hage Chahine and D. Fain, The mechanism of iron release from transferrin. Slow-proton-transfer-induced loss of nitrilotriacetatoiron(III) complex in acidic media, *Eur. J. Biochem.*, 1994, **223**, 581–587.
29 M. R. Ciriolo, A. Desideri, M. Paci and G. Rotilio, Reconstitution of Cu,Zn-superoxide dismutase by the Cu(I).glutathione complex, *J. Biol. Chem.*, 1990, **265**, 11030–11034.
30 P. M. Hanna, R. Tamilarasan and D. R. McMillin, Cu(I) analysis of blue copper proteins, *Biochem. J.*, 1988, **256**, 1001–1004.
31 H. Speisky, M. Gomez, C. Carrasco-Pozo, E. Pastene, C. Lopez-Alarcon and C. Olea-Azar, Cu(I)–glutathione complex: a potential source of superoxide radicals generation, *Bioorg. Med. Chem.*, 2008, **16**, 6568–6574.
32 Y. Zhang, E. R. Lyver, S. A. Knight, E. Lesuisse and A. Dancis, Frataxin and mitochondrial carrier proteins, Mrs3p and Mrs4p, cooperate in providing iron for heme synthesis, *J. Biol. Chem.*, 2005, **280**, 19794–19807.
33 R. Santos, A. Dancis, D. Eide, J. M. Camadro and E. Leuisse, Zinc suppresses the iron-accumulation phenotype of *Saccharomyces cerevisiae* lacking the yeast frataxin homologue (Yfh1), *Biochem. J.*, 2003, **375**, 247–254.
34 P. M. Schenk, S. Baumann, R. Mattes and H. H. Steinbiss, Improved high-level expression system for eukaryotic genes in *Escherichia coli* using T7 RNA polymerase and rare ArgtRNAs, *BioTechniques*, 1995, **19**, 196–198, 200.
35 F. W. Studier, Protein production by auto-induction in high density shaking cultures, *Protein Expression Purif.*, 2005, **41**, 207–234.
36 P. A. Cobine, F. Pierrel and D. R. Winge, Copper trafficking to the mitochondrion and assembly of copper metalloenzymes, *Biochim. Biophys. Acta*, 2006, **1763**, 759–772.
37 E. T. Zakharova, M. M. Shavlovski, M. G. Bass, A. A. Gridasova, M. O. Pulina, V. De Filippis, M. Beltramini, P. Di Muro, B. Salvato, A. Fontana, V. B. Vasilyev and V. S. Gaitskhoki, Interaction of lactoferrin with ceruloplasmin, *Arch. Biochem. Biophys.*, 2000, **374**, 222–228.
38 R. A. Binstead, A. D. Zuberbühler and B. Jung, *SPECFIT global analysis system version 3.04.34*, SPECFIT global analysis system version 30434, 2003.
39 H. J. Maple, O. Scheibner, M. Baumert, M. Allen, R. J. Taylor, R. A. Garlish, M. Bromirski and R. J. Burnley, Application of the Exactive Plus EMRfor automated protein–ligandscreening by non-covalent mass spectrometry, *Rapid Commun. Mass Spectrom.*, 2014, **28**, 1561–1568.
40 J. D. Cook, K. Z. Bencze, A. D. Jankovic, A. K. Crater, C. N. Busch, P. B. Bradley, A. J. Stemmler, M. R. Spaller and T. L. Stemmler, Monomeric Yeast Frataxin Is an Iron-Binding Protein, *Biochem. J.*, 2006, **45**, 7767–7777.
41 M. R. Ciriolo, M. Sette, M. Paci and G. Rotilio, A study of the intracellular effects of glutathione by 1H-spin echo NMR of intact human erythrocytes, *Biochem. Int.*, 1990, **20**, 397–403.
42 R. E. Barnett and W. P. Jencks, Diffusion-controlled proton transfer in intramolecular thiol ester aminolysis and thiazoline hydrolysis, *J. Am. Chem. Soc.*, 1969, **91**, 2358–2369.
43 E. Pines, B. Z. Magnes, M. J. Lang and G. R. Fleming, Direct measurement of intrinsic proton transfer rates in diffusion-controlled reactions, *Chem. Phys. Lett.*, 1997, **281**, 413–420.
44 C. Eid, M. Hemadi, N. T. Ha-Duong and J. M. El Hage Chahine, Iron uptake and transfer from ceruloplasmin to transferrin, *Biochim. Biophys. Acta*, 2014, **1840**, 1771–1781.
45 N. T. Ha-Duong, C. Eid, M. Hemadi and J. M. El Hage Chahine, In vitro interaction between ceruloplasmin and human serum transferrin, *Biochemistry*, 2010, **49**, 10261–10263.
46 M. Hemadi, P. H. Kahn, G. Miquel and J. M. El Hage Chahine, Transferrin's mechanism of interaction with receptor 1, *Biochemistry*, 2004, **43**, 1736–1745.
47 A. Seguin, A. Bayot, A. Dancis, A. Rogowska-Wrzesinska, F. Auchere, J. M. Camadro, A. L. Bulteau and E. Lesuisse, Overexpression of the yeast frataxin homolog (Yfh1): contrasting effects on iron–sulfur cluster assembly, heme synthesis and resistance to oxidative stress, *Mitochondrion*, 2009, **9**, 130–138.
48 V. Irazusta, E. Cabiscol, G. Reverter-Branchat, J. Ros and J. Tamarit, Manganese is the link between frataxin and iron–sulfur deficiency in the yeast model of Friedreich ataxia, *J. Biol. Chem.*, 2006, **281**, 12227–12232.
49 A. Seguin, R. Sutak, A. L. Bulteau, R. Garcia-Serres, J. L. Oddou, S. Lefevre, R. Santos, A. Dancis, J. M. Camadro, J. M. Latour and E. Lesuisse, Evidence that yeast frataxin is not an iron storage protein in vivo, *Biochim. Biophys. Acta*, 2010, **1802**, 531–538.
50 A. H. Koeppen, J. A. Morral, A. N. Davis, J. Qian, S. V. Petrocine, M. D. Knutson, W. M. Gibson, M. J. Cusack and D. Li, The dorsal root ganglion in Friedreich's ataxia, *Acta Neuropathol.*, 2009, **118**, 763–776.
51 S. Soriano, P. Calap-Quintana, J. V. Llorens, I. Al-Ramahi, L. Gutierrez, M. J. Martinez-Sebastian, J. Botas and M. D. Molto, Metal Homeostasis Regulators Suppress FRDA

Phenotypes in a Drosophila Model of the Disease, *PLoS One*, 2016, **11**, e0159209.
52 H. Kawamata and G. Manfedi, Import, maturation, and function of SOD1 and its copper chaperone CCS in the mitochondrial intermembrane space, *Antioxid. Redox Signaling*, 2010, **13**, 1375–1384.
53 N. J. Robinson and D. R. Winge, Copper metallochaperones, *Annu. Rev. Biochem.*, 2010, **79**, 537–562.
54 A. C. Rosenzweig and T. V. O'Halloran, Structure and chemistry of the copper chaperone proteins, *Curr. Opin. Chem. Biol.*, 2000, **4**, 140–147.
55 I. Gostimskaya and C. M. Grant, Yeast mitochondrial glutathione is an essential antioxidant with mitochondrial thioredoxin providing a back-up system, *Free Radical Biol. Med.*, 2016, **94**, 55–65.
56 C. Kumar, A. Igbaria, B. D'Autreaux, A. G. Planson, C. Junot, E. Godat, A. K. Bachhawat, A. Delaunay-Moisan and M. B. Toledano, Glutathione revisited: a vital function in iron metabolism and ancillary role in thiol-redox control, *EMBO J.*, 2011, **30**, 2044–2056.
57 M. B. Toledano, A. Delaunay-Moisan, C. E. Outten and A. Igbaria, Functions and cellular compartmentation of the thioredoxin and glutathione pathways in yeast, *Antioxid. Redox Signaling*, 2013, **18**, 1699–1711.
58 M. Mari, A. Morales, A. Colell, C. Garcia-Ruiz and J. C. Fernandez-Checa, Mitochondrial glutathione, a key survival antioxidant, *Antioxid. Redox Signaling*, 2009, **11**, 2685–2700.
59 R. Osterberg, R. Ligaarden and D. Persson, Copper(I) complexes of penicillamine and glutathione, *J. Inorg. Biochem.*, 1979, **10**, 341–355.
60 R. C. Hider and X. L. Kong, Glutathione: a key component of the cytoplasmic labile iron pool, *BioMetals*, 2011, **24**, 1179–1187.
61 A. L. Bulteau, S. Planamente, L. Jornea, A. Dur, E. Lesuisse, J. M. Camadro and F. Auchere, Changes in mitochondrial glutathione levels and protein thiol oxidation in yfh1 yeast cells and the lymphoblasts of patients with Friedreich's ataxia, *Biochim. Biophys. Acta*, 2012, **1822**, 212–225.
62 W. Qi, J. Li, C. Y. Chain, G. A. Pasquevich, A. F. Pasquevich and J. A. Cowan, Glutathione complexed Fe–S centers, *J. Am. Chem. Soc.*, 2012, **134**, 10745–10748.
63 L. Wang, B. Ouyang, Y. Li, Y. Feng, J. P. Jacquot, N. Rouhier and B. Xia, Glutathione regulates the transfer of iron–sulfur cluster from monothiol and dithiol glutaredoxins to apo ferredoxin, *Protein Cell*, 2012, **3**, 714–721.
64 T. L. Stemmler, E. Lesuisse, D. Pain and A. Dancis, Frataxin and mitochondrial FeS cluster biogenesis, *J. Biol. Chem.*, 2010, **285**, 26737–26743.
65 H. Yoon, R. Golla, E. Lesuisse, J. Pain, J. E. Donald, E. R. Lyver, D. Pain and A. Dancis, Mutation in the Fe–S scaffold protein Isu bypasses frataxin deletion, *Biochem. J.*, 2012, **441**, 473–480.
66 H. Yoon, S. A. Knight, A. Pandey, J. Pain, S. Turkarslan, D. Pain and A. Dancis, Turning *Saccharomyces cerevisiae* into a Frataxin-Independent Organism, *PLoS Genet.*, 2015, **11**, e1005135.
67 F. Prischi, P. V. Konarev, C. Iannuzzi, C. Pastore, S. Adinolfi, S. R. Martin, D. I. Svergun and A. Pastore, Structural bases for the interaction of frataxin with the central components of iron–sulphur cluster assembly, *Nat. Commun.*, 2010, **1**, 95.
68 A. Pandey, D. M. Gordon, J. Pain, T. L. Stemmler, A. Dancis and D. Pain, Frataxin directly stimulates mitochondrial cysteine desulfurase by exposing substrate-binding sites, and a mutant Fe–S cluster scaffold protein with frataxin-bypassing ability acts similarly, *J. Biol. Chem.*, 2013, **288**, 36773–36786.
69 H. Yoon, S. A. Knight, A. Pandey, J. Pain, Y. Zhang, D. Pain and A. Dancis, Frataxin-bypassing Isu1: characterization of the bypass activity in cells and mitochondria, *Biochem. J.*, 2014, **459**, 71–81.
70 A. Parent, X. Elduque, D. Cornu, L. Belot, J. P. Le Caer, A. Grandas, M. B. Toledano and B. D'Autreaux, Mammalian frataxin directly enhances sulfur transfer of NFS1 persulfide to both ISCU and free thiols, *Nat. Commun.*, 2015, **6**, 5686.
71 A. Pilotelle-Bunner, F. Cornelius, P. Sebban, P. W. Kuchel and R. J. Clarke, Mechanism of Mg2+ binding in the Na+,K+-ATPase, *Biophys. J.*, 2009, **96**, 3753–3761.
72 L. C. Thompson, S. Goswami, D. S. Ginsberg, D. E. Day, I. M. Verhamme and C. B. Peterson, Metals affect the structure and activity of human plasminogen activator inhibitor-1. I. Modulation of stability and protease inhibition, *Protein Sci.*, 2011, **20**, 353–365.